Electrochemical Studies of the Mono-Fe, Fe−Zn, and Fe−Fe Metalloisoforms of Bacteriophage λ Protein Phosphatase†

Tiffany A. Reiter* and Frank Rusnak‡

Section of Hematology Research and the Department of Biochemistry and Molecular Biology, Mayo Clinic and Foundation, Rochester, Minnesota 55905

Received September 19, 2003; Revised Manuscript Received November 18, 2003

ABSTRACT: Bacteriophage λ protein phosphatase (λPP) is a member of a large superfamily of metallophosphoesterases, including serine/threonine protein phosphatases, purple acid phosphatases, 5′-nucleotidase, and DNA repair enzymes such as Mre11. Members of this family share several common characteristics, including a common phosphoesterase motif, secondary structural fold (βαβαβ), and metal ligand environment, and often accommodate a dinuclear metal center. The identity of the active site metals often differs between family members. Despite the extensive spectroscopic studies of several family members, only the standard redox potential of porcine purple acid phosphate (PAP) has been measured. In this report, we investigate the redox properties of another member of this protein family. The standard redox potentials of the mono-Fe, Fe−Zn, and Fe−Fe metalloisoforms of λPP were determined from anaerobic redox titration experiments. Two different S = 5/2, mono-Fe^{3+} λPP species were identified: the first with an $E/D \approx 0.17$, $g = 8.9$ and 4.8, and an $E^{\circ\prime} \approx +130$ mV; the second with $E/D \approx 0.05$, $g = 6.7$, 5.9, and 4.4, and an $E^{\circ\prime} \approx +120$ mV. The first and second mono-Fe^{3+} species are thought to represent Fe present in the M2 and M1 sites, respectively. The addition of Zn^{2+} to mono-Fe^{3+} λPP results in a decrease in both mono-Fe^{3+} species and the appearance of a new S = 5/2, $Fe^{3+}-Zn^{2+}$ species ($E/D \approx 0.02$, $g =$ 5.9, and an $E^{\circ\prime} > +175$ mV). The Fe−Fe λPP titration revealed an S = 1/2, $Fe^{3+}-Fe^{2+}$ ($g < 2$) species with an $E^{\circ\prime} > +128$ mV. These results suggest that the active site of λPP supports a high oxidation potential for both metal sites and may indicate an equally oxidizing active site for other member metallophosphoesterases.

Bacteriophage λ protein phosphatase (λPP),[1] a 221-residue protein, was originally identified and characterized as a phosphatase by Cohen et al. on the basis of significant amino acid sequence homology with protein phosphatases 1 (PP1), 2A (PP2A), and 2B (PP2B, calcineurin) (*1*, *2*). One hundred fifteen residues of the N-terminus of λPP have 35, 35, and 25% sequence identity to the N-terminal sequences of PP1, PP2A, and calcineurin, respectively (*1*−*3*). λPP, PP1, PP2A, and calcineurin belong to a large family of metallophosphoesterases, which includes phosphatases from bacteria/cyanobacteria (*4*), archaea (*5*), yeast (*6*−*8*), protozoa (*9*), plants (*10*, *11*), and animals (*12*), as well as Mre11 nuclease (*13*), 5′-nucleotidase (*14*), and the purple acid phosphatases (PAP) (*15*−*19*). Members of this family share a common phosphoesterase motif, **D**X**H**(X)$_n$G**D**XXD(X)$_m$G**N**-H/DE (*20*−*22*). The residues in bold are situated in loops within a conserved secondary structural motif, the βαβαβ-fold, and are metal ligands to an active site dinuclear metal center (*13*, *14*, *23*−*28*). Mutagenesis has shown that several residues in the λPP phosphoesterase motif are required for metal binding, substrate binding, and catalytic activity (*21*, *29*). Similar results were observed following mutagenesis of PP1 (*30*), which suggests that family members also have a similar mechanism.

Despite these similarities in sequence and structure, each phosphatase in the family appears to have a different metal ion requirement. Different metalloisoforms of PAP have been purified from different animal and plant species: Fe−Fe, Fe−Zn, and Fe−Mn forms (*15*−*19*). PP1 and PP2A are activated by Mn^{2+}, Co^{2+}, and Fe^{2+}/ascorbate in vitro; however, the identity of the native metal ions has not been resolved (*31*−*35*). Calcineurin (PP2B), a Ca^{2+}/calmodulin-activated Fe−Zn enzyme, can also be activated in vitro by Mn^{2+} and Ni^{2+}, but there is no evidence to suggest that Mn^{2+} is an intrinsic metal activator (*36*−*43*). λPP and several other bacterial phosphatases are activated several-fold by addition of various metal ions in vitro, with Mn^{2+} and Ni^{2+} providing the most significant activation (*3*, *44*). An exchange coupled dinuclear-Mn^{2+} cluster has been observed for λPP using electron paramagnetic resonance (EPR) (*45*−*48*). λPP has also been reconstituted with iron to form an $Fe^{3+}-Fe^{2+}$ cluster (*29*), similar to those found in Fe-reconstituted calcineurin (*49*) and PAP (*50*).

† This work was supported by a grant from the National Institutes of Health (GM46865).

* To whom correspondence should be addressed at Harvard School of Public Health, Department of Genetics and Complex Diseases, 665 Huntington Ave 1-512, Boston, MA 02115. Tel: (617) 432-2501. Fax: (617) 432-0377. E-mail: treiter@hsph.harvard.edu.

‡ Deceased.

[1] Abbreviations: EPR, electron paramagnetic resonance; ICP-ES, inductively coupled plasma emission spectroscopy; IPTG, isopropyl-β-D-1-thiogalactopyranoside; λPP, bacteriophage lambda protein phosphatase; λPPpT7-7, T7 polymerase-based λPP-expression plasmid; NHE, normal hydrogen electrode; PAP, purple acid phosphatase; *p*NPP, *para*-nitrophenyl phosphate; PP1, protein phosphatase 1; PP2A, protein phosphatase 2A; PP2B, protein phosphatase 2B.

10.1021/bi0356956 CCC: $27.50
Published on Web 12/20/2003

Also of recent interest is the redox regulation of several members of the metallophosphoesterase superfamily. Evidence gathered both in vivo and in vitro suggests that calcineurin is redox regulated (*49*, *51*−*61*). Redox regulation of calcineurin was originally hypothesized based on the significant homology shared between calcineurin and plant PAP. Both enzymes have an $Fe^{3+}-Zn^{2+}$ cofactor and nearly identical ligand environment (*26*, *27*, *62*, *63*). PAPs require a mixed-valent $Fe^{3+}-M^{2+}$ (M = Fe, Zn) cluster for activity (assayed using *para*-nitrophenyl phosphate, *p*NPP) (*64*). Mammalian PAPs contain dinuclear $Fe^{3+}-Fe^{2+}$ clusters, in which an Fe^{2+} ion resides in a site identical to the Zn^{2+} ion in calcineurin (*65*). The Zn^{2+} ion of calcineurin can be substituted with Fe^{2+}, yielding a dinuclear $Fe^{3+}-Fe^{2+}$ cluster with nearly identical enzymatic properties to the $Fe^{3+}-Zn^{2+}$ form (*51*). Both the $Fe^{3+}-Zn^{2+}$ and $Fe^{3+}-Fe^{2+}$ forms of calcineurin have similar activities toward *p*NPP and a phosphopeptide substrate (*51*). Redox-dependent experiments with calcineurin demonstrated that only certain oxidation states retained catalytic activity toward *p*NPP. For the $Fe^{3+}-Zn^{2+}$ form of calcineurin, one electron reduction to the $Fe^{2+}-Zn^{2+}$ oxidation state rendered the enzyme inactive. A similar inactivation of the mixed-valent $Fe^{3+}-Fe^{2+}$ form of calcineurin occurred following either one electron reduction to the diferrous form ($Fe^{2+}-Fe^{2+}$) or one electron oxidation by H_2O_2 to the diferric ($Fe^{3+}-Fe^{3+}$) form of the enzyme (*49*). The requirement for a mixed-valent $Fe^{3+}-M^{2+}$ (M = Fe, Zn) cluster for calcineurin activity parallels the redox-dependent behavior observed for the PAPs (*64*). However, in contrast to these results, Namgaladze et al. purified calcineurin in the $Fe^{2+}-Zn^{2+}$ oxidation state and found that this form of the enzyme had slightly higher activity compared to the $Fe^{3+}-Zn^{2+}$ enzyme when a phosphopeptide was used as substrate (*60*). Further support for the $Fe^{2+}-Zn^{2+}$ oxidation state comes from earlier studies by Wang et al., which show that superoxide dismutase prevents calcineurin inactivation both in vitro and in vivo (*54*). Thus, there currently remains some controversy regarding the active oxidation state of calcineurin.

Despite the intensive study of the redox properties of calcineurin and PAP described above, the standard redox potential of only one family member has been accurately determined. The midpoint potential of porcine PAP was measured at +242 mV ($Fe^{3+}-Fe^{3+}/Fe^{3+}-Fe^{2+}$, pH = 7.0) (*66*). It is unknown whether all member phosphatases will have redox potentials similar to that of porcine PAP or if they will also support a mixed-valent metal oxidation state in their active sites ($Fe^{3+}-M^{2+}$, M = Fe, Zn) similar to that observed for PAPs and debated for calcineurin. Anaerobic redox titrations of mono-Fe, Fe−Zn, and Fe−Fe λPP were performed to investigate whether λPP will have a redox potential similar to porcine PAP and whether the λPP active site will support a mixed-valent metal oxidation state.

EXPERIMENTAL PROCEDURES

Materials. LB media was purchased from Fisher Scientific (Pittsburgh, PA). Ampicillin, $FeCl_3$, $K_3Fe(CN)_6$, $Na_2S_2O_4$, $ZnCl_2$, $Fe(NH_4)_2(SO_4)_2$, indigo tetrasulfonate, phenazine, 2-hydroxy-1,4-naphthoquinone, safranin O, benzyl viologen, methyl viologen, 2,6-dichloroindophenol, 1,2-naphthoquinone, phenazine methosulfate, 1,4-naphthoquinone, 5-hydroxy-1,4-naphthoquinone, methyl blue, duroquinone, and quinhydrone were purchased from Sigma Aldrich Chemical Co. (St. Louis, MO). DEAE Sephadex and phenyl Sepharose resins were purchased from Pharmacia (Piscataway, NJ). Isopropyl-β-D-1-thiogalactopyranoside (IPTG) was purchased from Bachem AG (Bubendorf, Switzerland). No-Chromix was purchased from Godax Laboratories Inc. (New York, NY). Competent cells of the *Escherichia coli* strain BL-21 Star (DE3)pLysS were purchased from Invitrogen (Carlsbad, CA). The λPP-expression plasmid (λPPpT7-7) contains the λPP gene upstream of the T7 polymerase promoter (*3*).

Overexpression of λPP in E. coli. The λPPpT7-7 plasmid was transformed into BL-21 Star (DE3)pLysS cells, and single colonies were used to inoculate 10 mL of Luria Bertani (LB) medium with ampicillin (0.1 mg/mL) for overnight culture at 37 °C. Overnight cultures were used to inoculate 1.5 L cultures of LB medium with ampicillin (0.1 mg/mL). These large cultures were grown at 37 °C until the OD_{600} was ≈ 1 (typically 6−7 h). Cultures were then induced with 1 mM IPTG and the temperature was lowered to 27 °C. After 21 h, the cells were harvested by centrifugation (3400*g*, 30 min). Cells were resuspended in 0.1 M Tris-Cl, pH 7.4, 1 mM EDTA (3 mL/g of cells). Cells were homogenized in an ice-cooled Bead Beater (Biospec Products Inc., Barlesville, OK) using 0.5-mm zirconia/silica beads with three, 1 min bursts of vortexing over a 10 min period to prevent overheating. Cell lysate was centrifuged at 39000*g* for 1 h, after which the supernatant was either used directly for protein purification or stored at −70 °C. The average yield of purified λPP per liter of λPPpT7-7 transformed BL-21 Star (DE3)pLysS cells was ≈ 50 mg.

Purification of λPP. Cell lysate supernatant was applied to a 500-mL column (diameter = 12.7 cm, height = 3.9 cm) of DEAE Sephadex CL-6B (Pharmacia, Piscataway, NJ) equilibrated in 25 mM Tris-Cl, pH 7.5, 1 mM EGTA. The column was washed with 3 vol of 25 mM Tris-Cl, pH 7.4, 1 mM EGTA, 20% glycerol and eluted with 25 mM Tris-Cl, pH 7.4, 1 mM EGTA, 0.1 M NaCl, 20% glycerol. The fractions (50 mL each) containing λPP were determined by electrophoresis on denaturing 12% polyacrylamide gels (SDS−PAGE). The fractions containing λPP were pooled, NaCl was added to 0.5 M, and the fractions applied to a 350-mL phenyl Sepharose column (diameter = 8.9 cm, height = 5.7 cm) (Pharmacia) equilibrated in 25 mM Tris-Cl, pH 7.4, 1 mM EGTA, 0.5 M NaCl. This column was then washed with 3 vol of equilibration buffer and 1 vol of 25 mM Tris-Cl, pH 7.4, and λPP eluted with 50 mM Tris-Cl, pH 7.5, 50% glycerol. The fractions containing pure λPP (as determined by SDS−PAGE) were pooled and concentrated to 11−27 mg/mL using a YM-10 ultrafiltration membrane in a Diaflow cell (Millipore, Bedford, MA). All purification procedures were performed at 4 °C.

Metalation of Apo-λPP. Purified λPP (50 mg) was dialyzed twice against 2 L of 50 mM Tris-Cl, pH 7.8, 100 mM NaCl, 10% glycerol. Following dialysis, the protein solution was placed in glass vials (No-Chromix/H_2SO_4-washed) and its volume was recorded. Two equivalents of Fe^{3+} (as a 50 mM solution of $FeCl_3$) was added to the apoprotein, and the sample was incubated for 3 h at 4 °C with slow stirring, and then concentrated to ≈1.6 mL using Centricon-10 ultrafiltration cells (Millipore). Excess Fe^{3+} was removed by passing the concentrated λPP over a NAP-25 gel filtration column (Pharmacia) using 100 mM Tris-Cl, pH 8.0 as the elution

buffer. Protein containing fractions were pooled and concentrated to ≈1.0 mL using Centricon-10 ultrafiltration cells. Fe analysis was performed using inductively coupled plasma emission spectroscopy (ICP-ES) in the Mayo Metals Laboratory and protein concentration was determined using the Coomassie Plus Protein Reagent (Pierce, Rockford, IL) using BSA as a standard. The resulting protein samples had a concentration of 1.00−1.44 mM and metal stoichiometries of 1.00−1.45 Fe/protein and were stored at −70 °C for later use in redox titration experiments.

The λPP pooled for the mono-Fe redox titrations had a concentration of 1.16 mM and an Fe/protein stoichiometry of 1.0.

Immmediately prior to redox titration experiments, 1 equiv of Zn^{2+} (added as $ZnCl_2$) or 4 equiv of Fe^{2+} (added as $Fe(NH_4)_2(SO_4)_2$) was added to the mono-Fe λPP to generate the Fe−Zn and Fe−Fe forms of λPP, respectively. The addition of 1 equiv of Zn^{2+} and 4 equiv of Fe^{2+} to mono-Fe^{3+} λPP resulted in optimal Fe^{3+}−Zn^{2+} and Fe^{3+}−Fe^{2+} cluster formation (data not shown).

Redox Titration Experiments. For each redox titration 3.5−4.0 mL of ≈1 mM mono-Fe^{3+} λPP was placed in a glass vial within an anaerobic glovebox (Labmaster 130, MBraun, Stratham, NH). A cocktail of redox mediators was prepared by mixing equal volumes of 3 mM stock solutions of 2,6-dichloroindophenol; 1,2-naphthoquinone; phenazine methosulfate; 1,4-naphthoquinone; 5-hydroxy-1,4-naphthoquinone; methyl blue; duroquinone; indigo tetrasulfonate; phenazine; 2-hydroxy-1,4-naphthoquinone; safranin O; benzyl viologen; and methyl viologen; resulting in a final concentration of 230 μM for each mediator. An aliquot of redox mediator cocktail was added to the λPP solution to a final concentration of 0.5% [λPP]. An Ag/AgCl working microelectrode (Microelectrodes Inc., Bedford, NH) and a Pt wire were first calibrated in a saturated quinhydrone solution ([benzoquinone]/[hydroquinone] (1:1), in pH 7 electrode buffer) prior to use. Potentials were measured using a Fluke 27 high-impedance digital multimeter (Fluke Biomedical). The potential versus normal hydrogen electrode (NHE) was determined by adding 287 mV (quinhydrone standard potential versus NHE) to the experimental potential. The potential of the protein solution was altered via successive additions (1 μL) of either 100 mM $K_3Fe(CN)_6$ (in 20 mM Tris-Cl, pH 7.6) or 20 mg/mL $Na_2S_2O_4$ (in 100 mM Tris-Cl, pH 9.0). At various potentials, an aliquot (250 μL) of protein was removed with a Hamilton syringe, placed in an EPR tube, immediately sealed with a rubber septum, removed from the glovebox, and frozen in liquid N_2. Throughout the titration, the protein solution was slowly stirred and maintained at 1 °C with use of a circulating cold bath.

EPR Spectroscopy. EPR spectra were recorded using a Bruker ESP 300E spectrometer operating at X-band microwave frequency (9.46 GHz) equipped with an Oxford Instruments ESR 900 continuous flow cryostat for cryogenic temperature regulation. Signal averaging to improve signal-to-noise was performed by averaging four scans for each sample.

EPR Data Quantitation and Modeling. The percentage of the mono-Fe λPP species with $E/D \approx 0.17$ in its oxidized state (mono-Fe^{3+}) in individual EPR spectra was determined by measurement of the peak-to-baseline intensity at 745.16 G ($g = 8.9$) and 4000.3 G normalized to 0% for the most reduced sample and 100% for the mean intensity of protein samples with $E \geq +207.6$ mV. The percentage of the mono-Fe λPP species with $E/D \approx 0.05$ in its oxidized state (mono-Fe^{3+}) in individual EPR spectra was determined by peak-to-baseline intensity at 1015 G ($g = 6.7$) and 4000.3 G normalized to 0% for the most reduced sample and 100% for the mean intensity of protein samples with $E \geq +207.6$ mV. Data from two independent titration experiments are shown. The relative intensity of the each mono-Fe^{3+} species versus experimental redox potential (mV vs NHE) was graphed and the data fitted with a Nernst curve ($R = 8.314$ J mol^{-1} K^{-1}, $T = 274.5$ K, $n = 1$, $F = 96\,494$ J V^{-1} mol^{-1}) with $E^{\circ\prime}$ of +130 mV and +120 mV for species with E/D of ≈0.17 and 0.05, respectively:

$$E = E^{\circ\prime} - \frac{RT}{nF}\ln(1 - [\text{oxidized}])/[\text{oxidized}]$$

The intensity of the EPR feature assigned to Fe^{3+}−Zn^{2+} λPP ($S = 5/2$, $E/D \approx 0.02$) in each individual EPR spectrum was determined by peak-to-baseline intensity at 1108.8 G ($g = 5.9$) and 4000.3 G, respectively. The percentage of the mono-Fe λPP species with $E/D \approx 0.17$ in its oxidized state (mono-Fe^{3+}) in EPR spectra from the Fe−Zn redox titration was determined by measurement of the peak-to-baseline intensity at 745.16 G ($g = 8.9$) and 4000.3 G normalized to 0% for the most reduced sample and 100% for the mean intensity of protein samples with $E \geq +175.0$ mV. The data were fit with a Nernst curve (described above) with an $E^{\circ\prime}$ of +130 mV (data not shown).

The intensity of the EPR feature attributed to Fe^{3+}−Fe^{2+} λPP ($S = 1/2$, $g < 2.0$) was quantitated for each individual spectrum by determining the peak-to-trough intensity at 3976.8 and 4252.5 G, respectively. Spin quantitation of the Fe^{3+}−Fe^{2+} λPP EPR signal in the $g = 2$ region was performed by comparison to a Cu-EDTA standard (*67*).

RESULTS

Measurement of the Redox Midpoint Potential of Two Mono-Fe λPP Species. Mono-Fe^{3+} λPP was prepared by addition of Fe^{3+} to the purified apoprotein, followed by rapid desalting to remove excess Fe^{3+}, and concentration of the protein sample as described in the methods section. Metal analysis of mono-Fe^{3+} protein samples gave Fe/protein stoichiometries ranging from 1 to 1.45. The pooled mono-Fe^{3+} λPP used for the two mono-Fe titrations had a metal stoichiometry of 1.0 Fe/protein. The EPR spectrum of mono-Fe^{3+} λPP (Figure 1) has resonances centered at $g = 8.9$, 6.7, 5.9, 4.8, 4.4, 4.3, and a broad shoulder feature from 1680 to 2000 G. Several of these resonances overlap in the region extending from 700 to 1500 G. The following reported g values correspond to two different high spin, $S = 5/2$, Fe^{3+} species: the first species with an $E/D \approx 0.17$ and $g = 8.9$ and 4.8: the second species with an $E/D \approx 0.05$ and $g =$ 6.7, 5.9, and 4.4. The $g = 4.3$ resonance represents adventitious Fe^{3+} iron present in the experiment.

EPR spectra of several mono-FeλPP samples poised at redox potentials from +400 to −200 mV (vs NHE) are shown in Figure 1. The spectra depicted were derived from two independent redox titration experiments, which utilized an identical pool of purified mono-Fe λPP (described above). In the first titration, the enzyme solution started at a potential

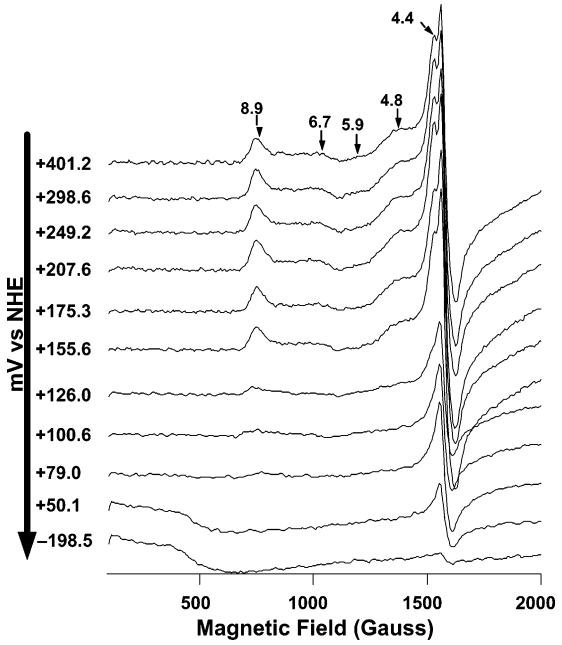

FIGURE 1: Selected EPR spectra from mono-Fe λPP redox titrations. EPR spectra (4 K) of mono-Fe λPP samples from two anaerobic redox titrations performed as described in the methods. Each spectrum was recorded under identical conditions: microwave frequency, 9.45 GHz; modulation amplitude and frequency, 2 G and 100 kHz; microwave power, 1.0 mW. The potential (vs NHE) for each protein sample is shown to the left of each spectrum. The g values of two different S = 5/2, mono-Fe^{3+} λPP species are indicated: the first with $g = 8.9$ and 4.8, and the second with $g = 6.7$, 5.9, and 4.4.

of +155.6 mV and was reduced in a stepwise fashion until the last sample was taken at −198.5 mV. The second titration began at +154.4 mV and was incrementally oxidized to +401.2 mV. The culmination of the two data sets resulted in a complete titration curve. Samples at potentials ≥ +126 mV exhibit resonances characteristic of both mono-Fe^{3+} λPP species, with a notable decrease in signal intensity as the potential falls below +150 mV. The loss of mono-Fe^{3+} signal resonances at lower potentials is expected due to reduction to the mono-Fe^{2+} oxidation state, an integer spin state (S = 2). The broad low field resonance (10−500 G) observed at potentials ≤ +50 mV is unlikely to represent such a mono-Fe^{2+}, S = 2 species and may result from either adventitious Fe or Fe^{2+} that has been exchanged from the active site to an external metal binding site. The relative quantity of each oxidized mono-Fe^{3+} species was determined by measurement of the intensity of the feature at $g = 8.9$ (745.16 G) and $g = 6.7$ (1015 G). The intensity of the most reduced sample and the mean intensity of the samples with $E \geq +207$ mV were normalized to represent 0 and 100% oxidized λPP, respectively. When the percentage of oxidized λPP (mono-Fe^{3+}) for each species is plotted versus potential (vs NHE), the data can be fitted with a Nernst curve with $E^{\circ\prime} = +130$ mV (Figure 2) and +120 mV (Figure 3) for the mono-Fe species with an E/D of ≈ 0.17 and 0.05, respectively.

Estimation of the Redox Midpoint Potential of Fe−Zn λPP. The Fe^{3+}−Zn^{2+} form of λPP was generated by addition of 1 equiv of Zn^{2+} to the mono-Fe^{3+} form of the enzyme (as described in the methods section). Several changes in the EPR spectrum of mono-Fe^{3+} λPP occur upon addition of Zn^{2+}: a loss of intensity at $g = 8.9$, 4.8, 4.4 and in the

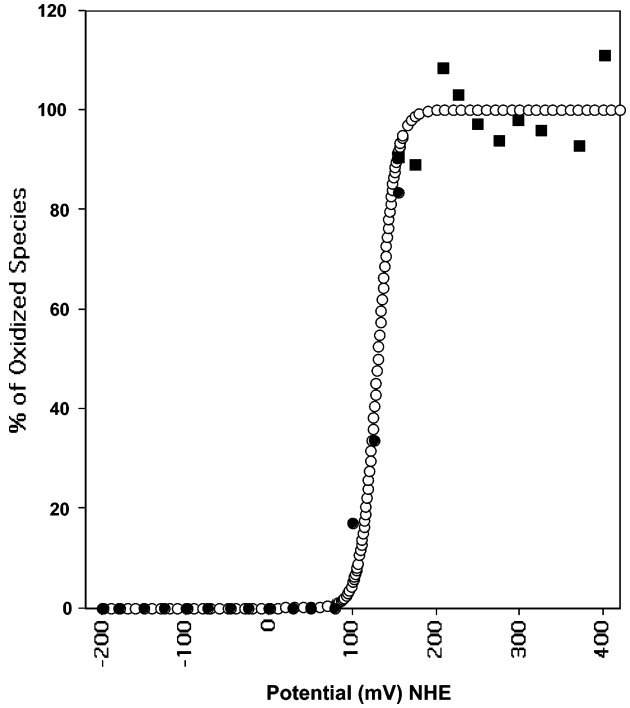

FIGURE 2: Standard redox potential of the S = 5/2, mono-Fe^{3+} species with $E/D \approx 0.17$. The EPR spectra from two mono-Fe redox titrations were analyzed as described in the methods. The percentage of the mono-Fe^{3+} λPP oxidation state versus potential (vs NHE) is shown for experiment A (●) and experiment B (■). A Nernst curve with $E^{\circ\prime} = +130$ mV is fit to the data (○).

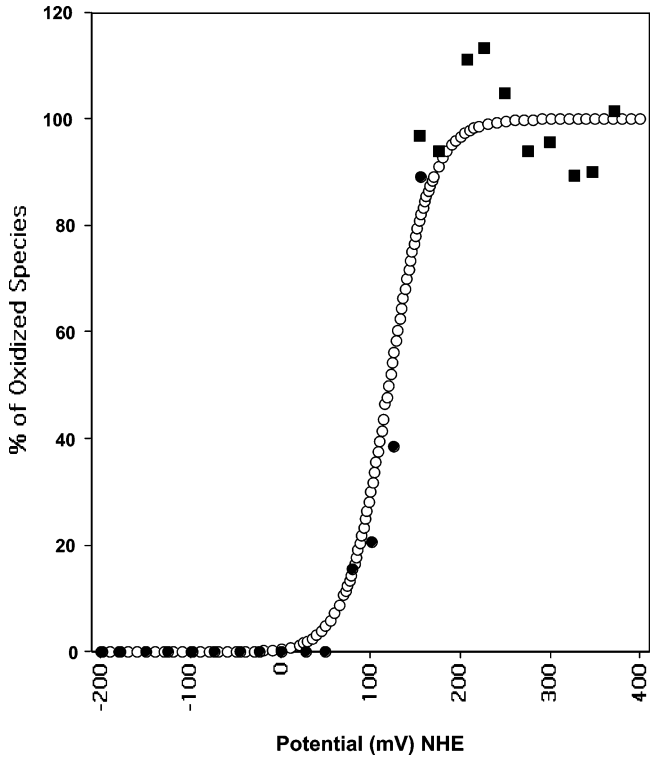

FIGURE 3: Standard redox potential of the S = 5/2, mono-Fe^{3+} species with $E/D \approx 0.05$. The EPR spectra from two mono-Fe redox titrations were analyzed as described in the methods. The percentage of the mono-Fe^{3+} λPP oxidation state versus potential (vs NHE) is shown for experiment A (●) and experiment B (■). A Nernst curve with $E^{\circ\prime} = +120$ mV is fit to the data (○).

shoulder feature from 1680 to 2000 G, and a notable increase in intensity at $g = 5.9$ (Figure 4). The changes in the

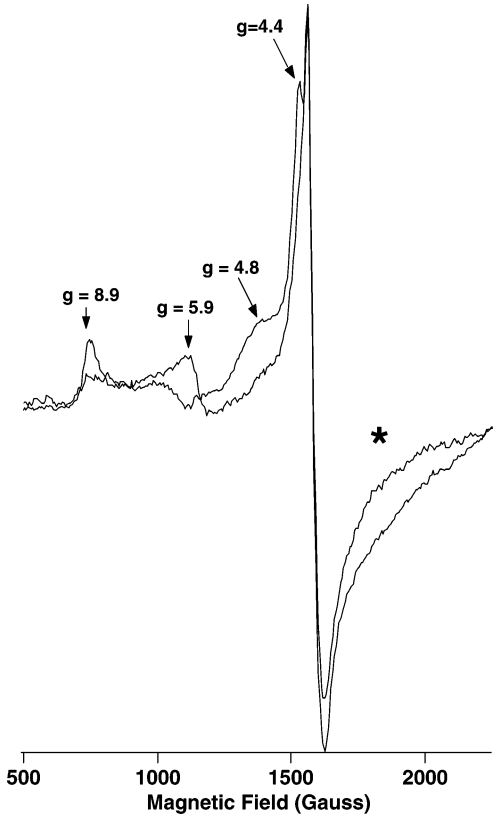

FIGURE 4: EPR spectrum of $Fe^{3+}-Zn^{2+}$ λPP. EPR spectra at 4 K of mono-Fe^{3+} λPP (solid) and $Fe^{3+}-Zn^{2+}$ (dotted line) λPP prepared as described in the methods. Spectra were recorded under the following conditions: microwave frequency, 9.45 GHz; modulation amplitude and frequency, 2 G and 100 kHz; microwave power, 1.0 mW. Relative to the mono-Fe^{3+} sample, the EPR spectrum of $Fe^{3+}-Zn^{2+}$ λPP has decreased intensity at $g = 8.9$, 4.8, 4.4, and the broad resonance feature extending from 1680 to 2140 G (asterisk), as well as an increase in intensity at $g = 5.9$.

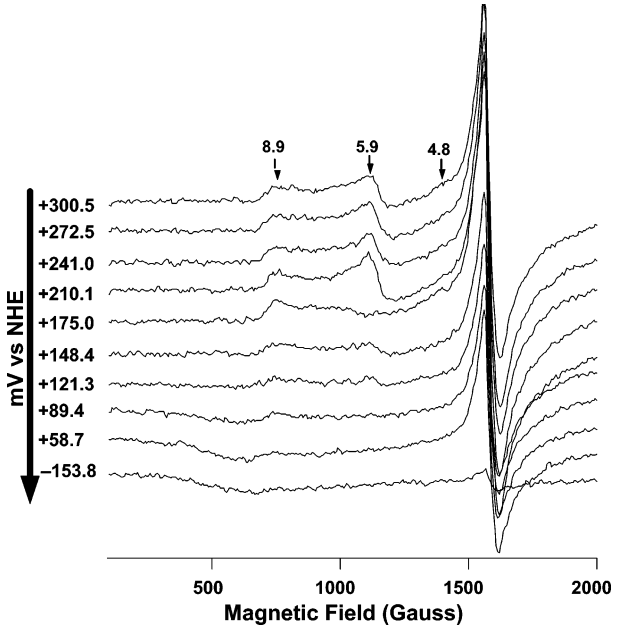

FIGURE 5: Selected EPR spectra from the Fe−Zn λPP redox titration. EPR spectra of Fe−Zn λPP samples from an anaerobic redox titration performed as described in Experimental Procedures. Each spectrum was recorded under identical conditions: temperature, 4 K; microwave frequency, 9.45 GHz; modulation amplitude and frequency, 2 G and 100 kHz; microwave power, 1.0 mW. The potential (vs NHE) is shown to the left of each spectrum. The g values characteristic of the mono-Fe^{3+} species with $E/D \approx 0.17$ ($g = 8.9$ and 4.8) and the $Fe^{3+}-Zn^{2+}$ species with $E/D \approx 0.02$ ($g = 5.9$) are indicated.

Table 1: Analysis of $Fe^{3+}-Zn^{2+}$ λPP Redox Titration EPR Data[a]

mV vs NHE	intensity of $g = 5.9$ EPR resonance feature ($\times 10^3$)
+210.1	87.4
+175.0	26.2
+89.4	13.3
+28.6	4.86
−27.2	0

[a] EPR spectra from the $Fe^{3+}-Zn^{2+}$ λPP redox titration were analyzed. The intensity of the $g = 5.9$ EPR feature was quantitated by determining the peak-to-baseline intensity at 1108.8 and 4000.3 G, respectively. The potential of each enzyme sample is shown in mV vs NHE.

spectrum indicate a loss of both mono-Fe species described above (E/D of ≈ 0.17 and 0.05) and formation of a new $Fe^{3+}-Zn^{2+}$ species ($S = 5/2$, $g = 5.9$, $E/D \approx 0.02$). A similar EPR spectrum has been described for $Fe^{3+}-Zn^{2+}$ calcineurin: with resonances at $g = 8.38$ and 5.69, representing a high-spin Fe^{3+} ($S = 5/2$) center (*51*). Comparative spectra have also been found for the $Fe^{3+}-Zn^{2+}$ forms of kidney bean purple acid phosphatase (*68*) and uteroferrin (*69*).

The EPR spectra of several samples of $Fe^{3+}-Zn^{2+}$ λPP poised at different potentials are shown in Figure 5. Samples buffered at potentials > +175 mV have spectra characteristic of both the mono-Fe species with $E/D \approx 0.17$ and $Fe^{3+}-Zn^{2+}$ λPP (all spectra not depicted in Figure 5). The $g = 5.9$ resonance corresponding to $Fe^{3+}-Zn^{2+}$ λPP is present at potentials > +175 mV, while resonances corresponding to the mono-Fe species persist at potentials > +58.7 mV. The loss of $g = 5.9$ signal intensity at potentials ≤ +175 mV is expected due to reduction of the $Fe^{3+}-Zn^{2+}$ λPP species to the $Fe^{2+}-Zn^{2+}$ oxidation state. The relative quantity of oxidized λPP ($Fe^{3+}-Zn^{2+}$) in each sample was determined by measurement of the peak-to-baseline intensity of the $g = 5.9$ resonance (1108.8 G), as described in Experimental Procedures. The intensity of the $g = 5.9$ resonance decreases significantly at potentials below +210 mV, suggesting an $E^{\circ\prime}$ > +175 mV (Table 1). When the intensity of the $g = 8.9$ feature corresponding to mono-Fe^{3+} λPP ($E/D \approx 0.17$) is plotted versus potential (vs NHE), the data can once again be fitted with a Nernst curve with $E^{\circ\prime} = +130$ mV (data not shown). The broad low field resonance (10 to 500 G) observed at potentials ≤ +89 mV is thought to again represent adventitious Fe or Fe^{2+} that has been equilibrium exchanged from the active site.

Estimation of the Redox Midpoint Potential of Fe−Fe λPP. The $Fe^{3+}-Fe^{2+}$ form of λPP was generated by the addition of 4 equiv of Fe^{2+} to the mono-Fe^{3+} form of the enzyme (as described in Experimental Procedures). The EPR spectrum of $Fe^{3+}-Fe^{2+}$ λPP has been previously reported and consists of a broad resonance feature extending from 3300 to 4000 G ($g < 2$) (Figure 6) (*29*). This resonance has been assigned to the spin-coupled binuclear $Fe^{3+}-Fe^{2+}$ center of Fe-reconstituted calcineurin (*51*), which has a ground state of $S = 1/2$ due to antiferromagnetic coupling between a high-spin Fe^{3+} ($S = 5/2$) and a high-spin Fe^{2+} ($S = 2$) ion. This characteristic EPR feature ($g < 2$) has been observed for a number of oxo-bridged dinuclear iron centers (*70, 71*).

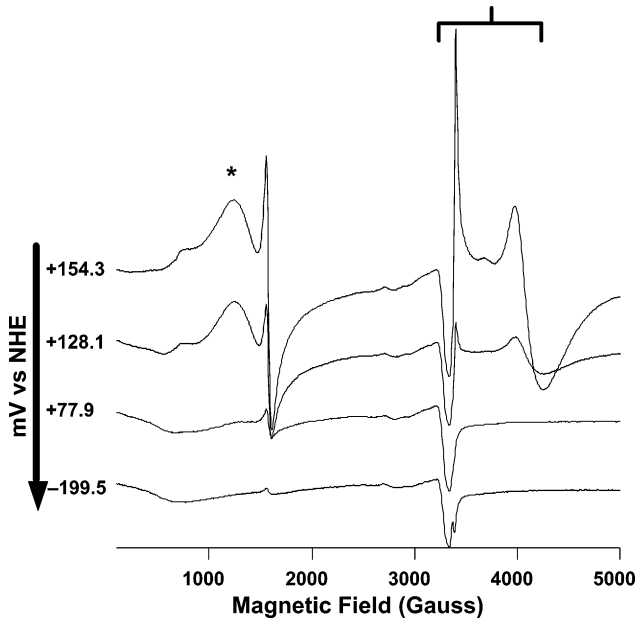

FIGURE 6: Selected EPR spectra from the Fe−Fe λPP redox titration. EPR spectra at 4 K of Fe−Fe λPP samples from an anaerobic redox titration performed as described in the methods. Each spectrum was recorded under identical conditions: microwave frequency, 9.45 GHz; modulation amplitude and frequency, 2 G and 100 kHz; microwave power, 1.0 mW. The potential (vs NHE) is shown to the left of each spectrum. The characteristic EPR feature from 3340 to 4250 G ($g < 2$) for $Fe^{3+}-Fe^{2+}$ λPP is indicated with a bracket. The resonance feature from 800 to 1400 G attributed to adventitiously bound Fe^{3+} and/or mono-Fe^{3+} λPP is indicated with an asterisk.

Select EPR spectra of an Fe−Fe λPP redox titration are shown in Figure 6. The titration depicted is an example of one experiment in which significant metalation of λPP to form the $Fe^{3+}-Fe^{2+}$ cluster was achieved (formation of $Fe^{3+}-Fe^{2+}$ λPP was not observed in all titration experiments). In this titration, samples with an $E > +128.1$ mV have spectra characteristic of $Fe^{3+}-Fe^{2+}$ λPP. The loss of the $g < 2$ resonance at potentials $< +128.1$ mV is expected, as $Fe^{2+}-Fe^{2+}$ λPP has an $S = 4$, integer spin state. The broad low field resonance at $E < +154$ mV has $S = 2$ character and is attributed to adventitious or equilibrium exchanged Fe^{2+} from the active site and is not likely to result from an $Fe^{2+}-Fe^{2+}$ λPP ($S = 4$) integer spin species. The broad signal present from 800 to 1400 G in samples with potentials $\geq +128.1$ mV is attributed to adventitiously bound Fe^{3+} and may also overlap any mono-Fe^{3+} λPP resonances present in the sample. Spin quantitation of the $Fe^{3+}-Fe^{2+}$ ($g < 2$) signal indicates that only ≈ 31% (0.44 mM) of the λPP present is in the Fe−Fe metalation state, with the remaining enzyme in the apo- or mono-Fe state. A similar resonance (500−1400 G) was observed in the EPR spectrum of $Fe^{3+}-Fe^{2+}$ calcineurin (*49*). The spectra also have an additional $g \approx 2$ resonance independent of the $Fe^{3+}-Fe^{2+}$ λPP species. This $g \approx 2$ species appears to increase in intensity as a function of potential and is attributed to a small amount of Cu present in the protein sample.

The intensity of the $Fe^{3+}-Fe^{2+}$ λPP EPR feature was quantitated by determination of the peak-to-trough intensity at 3976.8 and 4250 G, respectively (Table 2). A rapid increase in the signal intensity for $Fe^{3+}-Fe^{2+}$ λPP is observed in samples ranging from +77.9 to +154.3 mV, suggestive of an $E^{\circ\prime} > +128$ mV for this form of the enzyme.

Table 2: Analysis of $Fe^{3+}-Fe^{2+}$ λPP Redox Titration EPR Data[a]

mV vs NHE	intensity of S = 1/2 EPR resonance feature (× 10^3)
+154.3	667
+128.1	135
+77.9	2.49
−199.5	0

[a] EPR spectra from an $Fe^{3+}-Fe^{2+}$ λPP redox titration were analyzed. The intensity of the EPR feature representing $Fe^{3+}-Fe^{2+}$ λPP (3340 to 4250 G) was quantitated by determining the peak-to- trough intensity at 3976.8 and 4252.5 G, respectively. The potential of each enzyme sample is shown in mV vs NHE.

DISCUSSION

To characterize the redox properties of another member of the metallophosphoesterase superfamily, the standard redox potentials of the mono-Fe, Fe−Zn, and Fe−Fe metalloisoforms of λPP were determined. The mono-Fe λPP protein sample was prepared by addition of Fe^{3+} to the purified apoprotein, followed by rapid desalting to remove excess Fe^{3+}. Two anaerobic titrations were performed from a single λPP sample with an average metal stoichiometry of 1.0 Fe/molecule protein. The EPR spectrum of the mono-Fe λPP sample contained resonances corresponding to two distinct high spin ($S = 5/2$) Fe^{3+} species. The first species had resonances featured at $g = 8.9$ and 4.8 and an estimated E/D of 0.17. The second $S = 5/2$ species had an E/D of ≈ 0.05 and g values of 6.7, 5.9, and 4.4. Redox titration data resulted in measurement of a standard redox potential of approximately +130 and +120 mV for the species with E/D of ≈ 0.17 and 0.05, respectively. The two mono-Fe species are thought to result from Fe occupation of the individual M1 and M2 sites of λPP. Two similar $S = 5/2$, Fe^{3+} species were previously described for Fe−Zn calcineurin: the first with $g = 8.1$ and an $E/D \approx 0.11$ and the second with $g =$ 6.2 and 5.7 and near axial symmetry (*49*). The observance of similar spin species in λPP and calcineurin indicates a similarity in metal coordination geometry between these two members of the phosphoesterase family.

Assignment of the different mono-Fe spin states to either the M1 or M2 metal binding sites of λPP requires careful consideration. In the crystal structure by Voeglti et al., λPP accommodates two Mn^{2+} ions in its active site: each with six-coordinate geometry. Mn^{2+} at the M1 site has the following intermolecular distances (in angstroms) to its primary sphere of ligand atoms: H_2O, 2.6 (axial); Asp20, 2.4 (axial); Asp49, 2.2 (bridging); H_2O, 2.1 (bridging); H_2O, 2.3; and His22, 2.2 (*23*). Likewise, Mn^{2+} at the M2 site has the following intermolecular distances (in angstroms) to its ligand atoms: SO_4^{2-}, 2.4 (axial); His139, 2.2 (axial); Asp49, 2.3 (bridging); H_2O, 2.3 (bridging); His186, 2.2; and Asn75, 2.1. It is noted that the Mn^{2+} at the M1 site has a notably longer bond with its axially coordinated solvent molecule, compared to the corresponding bond found at the M2 site to SO_4^{2-} (2.6 versus 2.4 Å). This slight change in coordination geometry may allow the metal at the M1 site to have a lower rhombicity than that of the M2 site. In addition, the species corresponding to $E/D \approx 0.17$ appears to be the better populated of the two mono-Fe species. On the basis of the

significantly higher metal binding affinity of the M2 site ($k_D \approx \mu M$) relative to the affinity of the M1 site ($k_D \approx$ mM) (*47*), the majority of Fe in the sample is expected to occupy the M2 site. This fact also supports the assignment of the mono-Fe M1 and mono-Fe M2 states to the species with $E/D \approx 0.05$ and 0.17, respectively.

In addition to the two different mono-Fe^{3+} species mentioned above, there also appears to be a third species present in the mono-Fe λPP titration. This third species has a broad low field resonance (10−500 G) at potentials ≤ + 50 mV and has been attributed to adventitious iron or Fe^{2+} exchanged from the active site to an external site of the enzyme.

When 1 equiv of Zn^{2+} was added to the mono-Fe^{3+} λPP, several changes in the spectrum occurred. These spectral changes were attributed to loss of both mono-Fe species and formation of a new S = 5/2, $Fe^{3+}-Zn^{2+}$ cluster ($E/D \approx 0.02$ and $g = 5.9$). The presence of both mono-Fe and Fe−Zn λPP in the sample suggests that Zn metalation of mono-Fe λPP was incomplete. A similar EPR spectrum has been described for $Fe^{3+}-Zn^{2+}$ calcineurin: with resonances at $g = 8.38$ and 5.69, representing a high-spin Fe^{3+} (S = 5/2) center (*51*). The $Fe^{3+}-Zn^{2+}$ metalloisoforms of kidney bean PAP (*68*) and uteroferrin (*69*) also have comparative spectra. The Fe−Zn λPP species has an $E°' > +175$ mV. The mono-Fe species with E/D ≈ 0.17 was again measured to have an $E°' \approx +130$ mV. The K_D of the M1 and M2 site of λPP for Zn^{2+} is unknown, but Zn binds to sites corresponding to M2 in both PAP and calcineurin (*26*−*28*, *62*). The changes in the spectra suggest that Zn^{2+} occupies the M2 site of both mono-Fe species, resulting in displacement of the M2 Fe^{3+} and possible formation of a mono-Zn^{2+} center from the mono-Fe species with $E/D \approx 0.17$ and a new $Fe^{3+}-Zn^{2+}$ cluster derived from the mono-Fe species with $E/D \approx 0.05$. Also consistent with this hypothesis, is the slight change in symmetry of the mono-Fe^{3+} (S = 5/2) spin state which occurs upon addition of a Zn^{2+} ion at the M2 site ($E/D \approx$ 0.05 to 0.02, respectively).

The Fe−Zn metalloisoform had an increased standard redox potential relative to both mono-Fe species ($E°'$ of > +175 versus +120 and +130 mV). The observed difference in midpoint potentials was expected, as addition of a Zn^{2+} ion to the mono-Fe^{3+} active site would make a higher oxidation state of Fe more unfavorable (due to the high localization of positive charge in the active site) and thereby result in an increase in the standard redox potential ($E°'_{Fe-Zn} > E°'_{mono-Fe}$).

The Fe−Fe form of λPP was generated by addition of 4 equiv of Fe^{2+} to the mono-Fe^{3+} form of the enzyme. The EPR spectrum of the $Fe^{3+}-Fe^{2+}$ λPP formed corresponds to that previously reported (*29*) and consists of a broad resonance feature extending from 3300 to 4000 G ($g < 2$). The concentration of $Fe^{3+}-Fe^{2+}$ λPP in the titration was calculated to be 0.44 mM using spin quantitation with a Cu-EDTA standard, indicating that ≈ 31% of the original mono-Fe^{3+} λPP becomes fully metalated. The described $g < 2$ resonance is characteristic of the spin-coupled binuclear $Fe^{3+}-Fe^{2+}$ clusters of Fe-reconstituted calcineurin (*51*) and a number of other enzymes containing oxo-bridged diiron centers (*70*, *71*), which have a ground state of S = 1/2 due to antiferromagnetic coupling between a high-spin Fe^{3+} (S = 5/2) and a high-spin Fe^{2+} (S = 2) ion. The spectra from the titration indicate that the $E°'$ for $Fe^{3+}-Fe^{2+}$/ $Fe^{2+}-Fe^{2+}$ is > +128.1 mV. Again, the presence of an additional Fe ion in the active site is thought to increase the total positive charge in the active site, and thereby result in an increase in the standard redox potential of the Fe−Fe species relative to that of the mono-Fe species ($E°'$ of > +128 versus +120 and +130 mV).

The mono-Fe^{3+}, $Fe^{3+}-Zn^{2+}$, and $Fe^{3+}-Fe^{2+}$ metalloisoforms of λPP all appear to have $E°'$ values > +120 mV. The results suggest that the active site ligand environment of λPP provides a relatively oxidized environment for the active site metals. Several different members of the metallophosphoesterase family have been purified with a mixed valence ($Fe^{3+}-M^{2+}$) oxidation state including mammalian PAP (M = Fe) (*16*, *64*, *66*, *72*, *73*), sweet potato PAP (M = Mn or Zn) (*18*, *19*, *74*), soybean PAP (M = Zn) (*18*), kidney bean PAP (M = Zn) (*17*), and calcineurin (M = Zn) (*49*, *51*). However, it should be noted that calcineurin has recently been isolated in its reduced ($Fe^{2+}-Zn^{2+}$) oxidation state (in the presence of 5 mM ascorbate) (*60*). Despite the significant and important information gleaned from these spectroscopic studies, they do not provide an accurate assessment of a metal cluster's midpoint potential. Porcine PAP is the only member of the metallophosphoesterase family that has undergone careful electrochemical studies. Anaerobic redox titration studies of porcine PAP show the standard redox potential to be +242 mV ($Fe^{3+}-Fe^{3+}/Fe^{3+}-Fe^{2+}$, pH = 7.0) (*66*). On the basis of the conservation of the active site ligands (particularly at the M2 site), it is interesting to speculate that the redox potential of other members of the metallophosphoesterase family will also be > +100 mV. Anaerobic redox titration studies on other enzymes in this family will indicate whether standard redox potential is also a conserved feature between family members.

The λPP redox titration results also indicate that λPP would likely exist in the $M^{2+}-M^{2+}$ oxidation state in vivo. Despite knowledge that the physiological metal ion activator of λPP is Mn^{2+}, the results indicate that other metalloisoforms of λPP would exist in the $M^{2+}-M^{2+}$ oxidation state in the cytoplasm ($E = -230$ to -255 mV) (*75*−*78*). However, it is difficult to predict the in vivo oxidation state of a metal cluster based on reduction potentials measured in vitro. Phosphate (PO_4^{2-}), present in the cytosol, has been shown to significantly alter the reduction potential of porcine PAP in vitro: the standard redox potential of porcine PAP shifted by −193 mV in the presence of phosphate (*66*).

The requirement of a mixed-valent oxidation state of the PAPs ($Fe^{3+}-M^{2+}$, with M = Fe, Zn) (*79*) is consistent with the reduction potential measured for porcine PAP (+242 mV for $Fe^{3+}-Fe^{3+}/Fe^{3+}-Fe^{2+}$) (*66*). In contrast, other members of the metallophosphoesterase family have been purified in a reduced oxidation state ($M^{2+}-M^{2+}$, M = Mn or Zn) and therefore do not appear to require a mixed-valent oxidation state for catalysis: $Mn^{2+}-Mn^{2+}$ for λPP and Mre11 (*13*, *23*, *46*, *47*) and $Zn^{2+}-Zn^{2+}$ for 5′-nucleotidase (*14*). The active oxidation state of calcineurin is presently debated in the literature with different groups proposing an active $Fe^{3+}-Zn^{2+}$ or $Fe^{2+}-Zn^{2+}$ metal cluster (*49*, *51*, *54*, *60*). Future anaerobic redox titration experiments on calcineurin will help predict which oxidation state of the metal cluster is present in vivo and whether a mixed-valent oxidation state is required for activity.

ACKNOWLEDGMENT

This article is dedicated to Frank Rusnak, and his wife and young son, Rae and Leo. Special thanks to Jose Moura, Isabel Moura, and Carla Ascenso for instruction on anaerobic redox titrations and to Thomas Burghardt, Whyte Owen, Nancy Wengenack, Gang Xing, Françoise Auchere, and Reza Ghiladi for their careful review of the manuscript and the reviewers for their thoughtful comments.

REFERENCES

1. Cohen, P., and Cohen, P. T. W. (1989) Protein phosphatases come of age. *J. Biol. Chem. 264*, 21435−21438.
2. Cohen, P. T., Collins, J. F., Coulson, A. F., Berndt, N., and da Cruz e Silva, O. B. (1988) Segments of bacteriophage lambda (orf 221) and phi 80 are homologous to genes coding for mammalian protein phosphatases. *Gene 69*, 131−134.
3. Zhuo, S., Clemens, J. C., Hakes, D. J., Barford, D., and Dixon, J. E. (1993) Expression, purification, crystallization, and biochemical characterization of a recombinant protein phosphatase. *J. Biol. Chem. 268*, 17754−17761.
4. Missiakas, D., and Raina, S. (1997) Signal transduction pathways in response to protein misfolding in the extracytoplasmic compartments of *E.coli*: role of two new phosphoprotein phosphatases PrpA and PrpB. *EMBO J. 16*, 1670−1685.
5. Mai, B., Frey, G., Swanson, R. V., Mathur, E. J., and Stetter, K. O. (1998) Molecular cloning and functional expression of a protein-serine/threonine phosphatase from the hyperthermophilic archaeon *Pyrodictium abyssi* TAG11. *J. Bacteriol. 180*, 4030−4035.
6. Liu, Y., Ishii, S., Tokai, M., Tsutsumi, H., Ohki, O., Akada, R., Tanaka, K., Tsuchiya, E., Fukui, S., and Miyakawa, T. (1991) The *Saccharomyces cerevisiae* genes (CMP1 and CMP2) encoding calmodulin-binding proteins homologous to the catalytic subunit of mammalian protein phosphatase 2B. *Mol. Gen. Genet. 227*, 52−59.
7. Cyert, M. S., Kunisawa, R., Kaim, D., and Thorner, J. (1991) Yeast has homologs (CNA1 and CNA2 gene products) of mammalian calcineurin, a calmodulin-regulated phosphoprotein phosphatase. *Proc. Nat. Acad. Sci. U.S.A. 88*, 7376−7380.
8. Higuchi, S., Tamura, J., Giri, P. R., Polli, J. W., and Kincaid, R. L. (1991) Calmodulin-dependent protein phosphatase from *Neurospora crassa*. Molecular cloning and expression of recombinant catalytic subunit. *J. Biol. Chem. 266*, 18104−18112.
9. Garcia, A., Cayla, X., Barik, S., and Langsley, G. (1999) A family of PP2 phosphatases in *Plasmodium falciparum* and parasitic protozoa. *Parasitol. Today 15*, 90−92.
10. Smith, R. D., and Walker, J. C. (1996) Plant protein phosphatases. *Annu. Rev. Plant Physiol. Plant Mol. Biol. 47*, 101−125.
11. Luan, S. (1998) Protein phosphatases and signalling cascades in higher plants. *Trends Plant Sci. 3*, 271−275.
12. Rusnak, F., and Mertz, P. (2000) Calcineurin: form and function. *Physiol. Rev. 80*, 1483−1521.
13. Hopfner, K. P., Karcher, A., Craig, L., Woo, T. T., Carney, J. P., and Tainer, J. A. (2001) Structural biochemistry and interaction architecture of the DNA double-strand break repair Mre11 nuclease and Rad50-ATPase. *Cell 105*, 473−485.
14. Knöfel, T., and Sträter, N. (1999) X-ray structure of the *Escherichia coli* periplasmic 5′-nucleotidase containing a dimetal catalytic site. *Nature Struct. Biol. 6*, 448−453.
15. Campbell, H. D., Dionysius, D. A., Keough, D. T., Wilson, B. E., de Jersey, J., and Zerner, B. (1978) Iron-containing acid phosphatases: comparison of the enzymes from beef spleen and pig allantoic fluid. *Biochem. Biophys. Res. Commun. 82*, 615−620.
16. Davis, J. C., and Averill, B. A. (1982) Evidence for a spin-coupled binuclear iron unit at the active site of the purple acid phosphatase from beef spleen. *Proc. Nat. Acad. Sci. U.S.A. 79*, 4623−4627.
17. Beck, J. L., McConachie, L. A., Summors, A. C., Arnold, W. N., de Jersey, J., and Zerner, B. (1986) Properties of a purple acid phosphatase from red kidney bean: a zinc−iron metalloenzyme. *Biochim. Biophys. Acta 869*, 61−68.
18. Schenk, G., Ge, Y., Carrington, L. E., Wynne, C. J., Searle, I. R., Carroll, B. J., Hamilton, S., and de Jersey, J. (1999) Binuclear metal centers in plant purple acid phosphatases: Fe−Mn in sweet potato and Fe−Zn in soybean. *Arch. Biochem. Biophys. 370*, 183−189.
19. Schenk, G., Boutchard, C. L., Carrington, L. E., Noble, C. J., Moubaraki, B., Murray, K. S., de Jersey, J., Hanson, G. R., and Hamilton, S. (2001) A purple acid phosphatase from sweet potato contains an antiferromagnetically coupled binuclear Fe−Mn center. *J. Biol. Chem. 276*, 19084−19088.
20. Koonin, E. (1994) Conserved sequence pattern in a wide variety of phosphoesterases, *Protein Sci. 3*, 356−358.
21. Zhuo, S., Clemens, J. C., Stone, R. L., and Dixon, J. E. (1994) Mutational analysis of a Ser/Thr phosphatase. Identification of residues important in phosphoesterase substrate binding and catalysis. *J. Biol. Chem. 269*, 26234−26238.
22. Lohse, D. L., Denu, J. M., and Dixon, J. E. (1995) Insights derived from the structures of the Ser/Thr phosphatases calcineurin and protein phosphatase 1. *Structure 3*, 987−990.
23. Voegtli, W. C., White, D. J., Reiter, N. J., Rusnak, F., and Rosenzweig, A. C. (2000) Structure of the bacteriophage lambda Ser/Thr protein phosphatase with sulfate ion bound in two coordination modes. *Biochemistry 39*, 15365−15374.
24. Goldberg, J., Huang, H. B., Kwon, Y. G., Greengard, P., Nairn, A. C., and Kuriyan, J. (1995) Three-dimensional structure of the catalytic subunit of protein serine/threonine phosphatase-1. *Nature 376*, 745−753.
25. Egloff, M. P., Cohen, P. T., Reinemer, P., and Barford, D. (1995) Crystal structure of the catalytic subunit of human protein phosphatase 1 and its complex with tungstate. *J. Mol. Biol. 254*, 942−959.
26. Griffith, J. P., Kim, J. L., Kim, E. E., Sintchak, M. D., Thomson, J. A., Fitzgibbon, M. J., Fleming, M. A., Caron, P. R., Hsiao, K., and Navia, M. A. (1995) X-ray structure of calcineurin inhibited by the immunophilin-immunosuppressant FKBP12−FK506 complex. *Cell 82*, 507−522.
27. Kissinger, C. R., Parge, H. E., Knighton, D. R., Lewis, C. T., Pelletier, L. A., Tempczyk, A., Kalish, V. J., Tucker, K. D., Showalter, R. E., Moomaw, E. W., Gastinel, L. N., Habuka, N., Chen, X., Maldonado, F., Barker, J. E., Bacquet, R., and Villafranca, J. E. (1995) Crystal structures of human calcineurin and the human FKBP12-FK506-calcineurin complex. *Nature 378*, 641−644.
28. Sträter, N., Klabunde, T., Tucker, P., Witzel, H., and Krebs, B. (1995) Crystal structure of a purple acid phosphatase containing a dinuclear Fe(III)-Zn(II) active site. *Science 268*, 1489−1492.
29. Mertz, P., Yu, L., Sikkink, R., and Rusnak, F. (1997) Kinetic and spectroscopic analyses of mutants of a conserved histidine in the metallophosphatases calcineurin and lambda protein phosphatase. *J. Biol. Chem. 272*, 21296−21302.
30. MacKintosh, C., and MacKintosh, R. W. (1994) Inhibitors of protein kinases and phosphatases. *Trends Biochem. Sci. 19*, 444−448.
31. Hubbard, M. J., and Cohen, P. (1993) On target with a new mechanism for the regulation of protein phosphorylation. *Trends Biochem. Sci. 18*, 172−177.
32. Chu, Y., Lee, E. Y., and Schlender, K. K. (1996) Activation of protein phosphatase 1. Formation of a metalloenzyme. *J. Biol. Chem. 271*, 2574−2577.
33. Chu, Y., Wilson, S. E., and Schlender, K. K. (1994) A latent form of protein phosphatase 1 alpha associated with bovine heart myofibrils. *Biochim. Biophys. Acta 1208*, 45−54.
34. Yu, J. S., Chan, W. H., and Yang, S. D. (1996) Activation of the ATP·Mg-dependent type 1 protein phosphatase by the Fe^{2+}/ascorbate system. *J. Prot. Chem. 15*, 455−460.
35. Cai, L., Chu, Y., Wilson, S. E., and Schlender, K. K. (1995) A metal-dependent form of protein phosphatase 2A. *Biochem. Biophys. Res. Comm. 208*, 274−279.
36. Pallen, C. J., and Wang, J. H. (1983) Calmodulin-stimulated dephosphorylation of *p*-nitrophenyl phosphate and free phosphotyrosine by calcineurin. *J. Biol. Chem. 258*, 8550−8553.
37. Pallen, C. J., and Wang, J. H. (1984) Regulation of calcineurin by metal ions. Mechanism of activation by Ni^{2+} and an enhanced response to Ca^{2+}/calmodulin. *J. Biol. Chem. 259*, 6134−6141.
38. Pallen, C. J., and Wang, J. H. (1986) Stoichiometry and dynamic interaction of metal ion activators with calcineurin phosphatase. *J. Biol. Chem. 261*, 16115−16120.
39. King, M. M., and Huang, C. Y. (1984) The calmodulin-dependent activation and deactivation of the phosphoprotein phosphatase, calcineurin, and the effect of nucleotides, pyrophosphate, and

divalent metal ions. Identification of calcineurin as a Zn and Fe metalloenzyme. *J. Biol. Chem. 259*, 8847−8856.
40. Wolff, D. J., and Sved, D. W. (1985) The divalent cation dependence of bovine brain calmodulin-dependent phosphatase. *J. Biol. Chem. 260*, 4195−4202.
41. Li, H. C. (1984) Activation of brain calcineurin phosphatase towards nonprotein phosphoesters by Ca^{2+}, calmodulin, and Mg^{2+}. *J. Biol. Chem. 259*, 8801−8807.
42. King, M. M., and Huang, C. Y. (1983) Activation of calcineurin by nickel ions. *Biochem. Biophys. Res. Commun. 114*, 955−961.
43. Gupta, R. C., Khandelwal, R. L., and Sulakhe, P. V. (1984) Intrinsic phosphatase activity of bovine brain calcineurin requires a tightly bound trace metal. *FEBS Lett. 169*, 251−255.
44. Shi, L., Kehres, D. G., and Maguire, M. E. (2001) The PPP-family protein phosphatases PrpA and PrpB of *Salmonella enterica* serovar Typhimurium possess distinct biochemical properties. *J. Bacteriol. 183*, 7053−7057.
45. Reiter, N. J., White, D. J., and Rusnak, F. (2002) Inhibition of bacteriophage lambda protein phosphatase by organic and oxoanion inhibitors. *Biochemistry 41*, 1051−1059.
46. Rusnak, F., Yu, L., Todorovic, S., and Mertz, P. (1999) Interaction of bacteriophage lambda protein phosphatase with Mn(II): evidence for the formation of a $[Mn(II)]_2$ cluster. *Biochemistry 38*, 6943−6952.
47. White, D. J., Reiter, N. J., Sikkink, R. A., Yu, L., and Rusnak, F. (2001) Identification of the high affinity Mn^{2+} binding site of bacteriophage lambda phosphoprotein phosphatase: effects of metal ligand mutations on electron paramagnetic resonance spectra and phosphatase activities. *Biochemistry 40*, 8918−8929.
48. Reiter, T. A., Reiter, N. J., and Rusnak, F. (2002) Mn^{2+} is a native metal ion activator for bacteriophage lambda protein phosphatase. *Biochemistry 41*, 15404−15409.
49. Yu, L., Golbeck, J., Yao, J., and Rusnak, F. (1997) Spectroscopic and enzymatic characterization of the active site dinuclear metal center of calcineurin: implications for a mechanistic role. *Biochemistry 36*, 10727−10734.
50. Klabunde, T., and Krebs, B. (1997) The dimetal center in purple acid phosphatase. *Struct. Bonding 89*, 177−198.
51. Yu, L., Haddy, A., and Rusnak, F. (1995) Evidence that calcineurin accommodates an active site binuclear metal center. *J. Am. Chem. Soc. 117*, 10147−10148.
52. Bogumil, R., Namgaladze, D., Schaarschmidt, D., Schmachtel, T., Hellstern, S., Mutzel, R., and Ullrich, V. (2000) Inactivation of calcineurin by hydrogen peroxide and phenylarsine oxide. Evidence for a dithiol−disulfide equilibrium and implications for redox regulation. *Eur. J. Biochem. 267*, 1407−1415.
53. Reiter, T. A., Abraham, R. T., Choi, M., and Rusnak, F. (1999) Redox regulation of calcineurin in T-lymphocytes. *J. Biol. Inorg. Chem. 4*, 632−644.
54. Wang, X., Culotta, V. C., and Klee, C. B. (1996) Superoxide dismutase protects calcineurin from inactivation. *Nature 383*, 434−437.
55. El-Hag, A., and Clark, R. A. (1987) Immunosuppression by activated human neutrophils. Dependence on the myeloperoxidase system. *J. Immunol. 139*, 2406−2413.
56. Furuke, K., Shiraishi, M., Mostowski, H. S., and Bloom, E. T. (1999) Fas ligand induction in human NK cells is regulated by redox through a calcineurin-nuclear factors of activated T cell-dependent pathway. *J. Immunol. 162*, 1988−1993.
57. Sommer, D., Fakata, K. L., Swanson, S. A., and Stemmer, P. M. (2000) Modulation of the phosphatase activity of calcineurin by oxidants and antioxidants in vitro. *Eur. J. Biochem. 267*, 2312−2322.
58. Ferri, A., Gabbianelli, R., Casciati, A., Paolucci, E., Rotilio, G., and Carri, M. T. (2000) Calcineurin activity is regulated both by redox compounds and by mutant familial amyotrophic lateral sclerosis-superoxide dismutase. *J. Neurochem. 75*, 606−613.
59. Carballo, M., Márquez, G., Conde, M., Martín-Nieto, J., Monteseirín, J., Conde, J., Pintado, E., and Sobrino, F. (1999) Characterization of calcineurin in human neutrophils. Inhibitory effect of hydrogen peroxide on its enzyme activity and on NF-kappaB DNA binding. *J. Biol. Chem. 274*, 93−100.
60. Namgaladze, D., Hofer, H. W., and Ulrich, V. (2002) Redox control of calcineurin by targeting the binuclear Fe^{2+}-Zn^{2+} center at the enzyme active site. *J. Biol. Chem. 277*, 5962−5969.
61. Reiter, T. A., and Rusnak, F. (2002) Is calcineurin a peroxide-specific sensor in T-lymphocytes. *J. Biol. Inorg. Chem. 7*, 823−834.
62. Klabunde, T., Sträter, N., Fröhlich, R., Witzel, H., and Krebs, B. (1996) Mechanism of Fe(III)-Zn(II) purple acid phosphatase based on crystal structure. *J. Mol. Biol. 259*, 737−748.
63. Uppenberg, J., Lindqvist, F., Svensson, C., Ek-Rylander, B., and Andersson, G. (1999) Crystal structure of a mammalian purple acid phosphatase. *J. Mol. Biol. 290*, 201−211.
64. Merkx, M., and Averill, B. A. (1998) The activity of oxidized bovine spleen purple acid phosphatase is due to an Fe(III)Zn(II) 'impurity'. *Biochemistry 37*, 11223−11231.
65. Rusnak, F., Yu, L., and Mertz, P. (1996) Metalloenzymes and signal transduction: the protein serine/threonine phosphatases, a novel class of binuclear metal-containing enzymes. *J. Biol. Inorg. Chem. 1*, 388−396.
66. Wang, D. L., Holz, R. C., David, S. S., Que, L., Jr., and Stankovich, M. T. (1991) Electrochemical properties of the diiron core of uteroferrin and its anion complexes. *Biochemistry 30*, 8187−8194.
67. Orme-Johnson, N. R., and Orme-Johnson, W. H. (1978) Detection and quantitation of free cytochrome P-450 and cytochrome P-450 complexes by EPR spectroscopy. *Methods Enzmol. 52*, 252−257.
68. Beck, J. L., de Jersey, J., Zerner, B., Hendrich, M. P., and Debrunner, P. G. (1988) Properties of the Fe(II)-Fe(III) derivative of red kidney bean purple phosphatase. Evidence for a binuclear zinc−iron center in the native enzyme. *J. Am. Chem. Soc. 110*, 3317−3318.
69. David, S. S., and Que, L., Jr. (1990) Anion binding to uteroferrin. Evidence for phosphate coordination to the iron(III) ion of the dinuclear active site and interaction with the hydroxo bridge. *J. Am. Chem. Soc. 112*, 6455−6463.
70. Kurtz, D. M., Jr. (1990) Oxo- and hydroxo- bridged diiron complexes: a chemical perspective on a biological unit. *Chem. Rev. 90*, 585−606.
71. Vincent, J. B., Olivier-Lilley, G., and Averill, B. (1990) Proteins containing oxo-bridged dinuclear iron centers: a bioinorganic perspective. *Chem. Rev. 90*, 1447−1467.
72. Orlando, J. L., Zirino, T., Quirk, B. J., and Averill, B. A. (1993) Purification and properties of the native form of the purple acid phosphatase from bovine spleen. *Biochemistry 32*, 8120−8129.
73. Crowder, M. W., Vincent, J. B., and Averill, B. A. (1992) Electron paramagnetic resonance studies on the high-salt form of bovine spleen purple acid phosphatase. *Biochemistry 31*, 9603−9608.
74. Durmus, A., Eicken, C., Sift, B. H., Kratel, A., Kappl, R., Hüttermann, J., and Krebs, B. (1999) The active site of purple acid phosphatase from sweet potatoes (*Ipomoea batatas*): metal content and spectroscopic characterization. *Eur. J. Biochem. 260*, 709−716.
75. Williamson, D. H., Lund, P., and Krebs, H. A. (1967) The redox state of free nicotinamide-adenine dinucleotide in the cytoplasm and mitochondria of rat liver. *Biochem. J. 103*, 514−527.
76. Veech, R. L., Guynn, R., and Veloso, D. (1972) The time-course of the effects of ethanol on the redox and phosphorylation states of rat liver. *Biochem. J. 127*, 387−397.
77. Gilbert, H. F. (1990) Molecular and cellular aspects of thiol-disulfide exchange. *Adv. Enzymol. Relat. Areas Mol. Biol. 63*, 69−172.
78. Hwang, C., Sinskey, A. J., and Lodish, H. F. (1992) Oxidized redox state of glutathione in the endoplasmic reticulum. *Science 257*, 1496−1502.
79. Merkx, M., and Averill, B. A. (1998) Ga^{3+} as a functional substitute for Fe^{3+}: preparation and characterization of the Ga^{3+}-Fe^{2+} and $Ga^{3+}Zn^{2+}$ forms of bovine spleen purple acid phosphatase. *Biochemistry 37*, 8490−8497.

BI0356956